

Reliable and Computationally Affordable Prediction of the Energy Gap of Realistic TiO₂ Nanoparticles from Density Functional Theory†

Ángel Morales-García, Rosendo Valero, Francesc Illas*

Departament de Ciència de Materials i Química Física & Institut de Química Teòrica i Computacional (IQTCUB), Universitat de Barcelona. c/ Martí i Franquès 1, 08028 Barcelona, Spain

Abstract

The optical gap (O_{gap}) of a set $(\text{TiO}_2)_n$ nanoclusters and nanoparticles with $n = 10\text{--}286$ and different morphologies such as spherical, octahedral, lamellar, or tubular finite structures is investigated based on a relativistic all-electron description along with numerical atomic centered orbital basis set. Two different functionals are used, PBE and PBEx, the former corresponds to a standard implementation of the Generalized Gradient Approach (GGA) and the latter to a hybrid functional with 12.5% of Fock exchange which reproduces the band gap of bulk TiO₂ anatase and rutile. It is shown that the inclusion of exchange Fock in the PBE functional promotes a systematic energy gap opening of 1.25 eV relative to the PBE values. Remarkably, a linear correlation is found between PBEx and PBE O_{gap} calculated values with concomitant similar correlations for the HOMO and LUMO orbital energies. However, it appears that PBEx induces a larger downshift on the HOMO orbital than the upshift observed on the LUMO one. The fact that PBEx hybrid functional was shown to reproduce the experimental energy gaps of stoichiometric and reduced TiO₂ bulk phases leads to a suitable and practical way to successfully estimate O_{gap} of realistic TiO₂ nanoparticles composed by thousands of atoms with PBEx precision from computationally affordable PBE calculations.

E-mail: francesc.illas@ub.edu

† Electronic supplementary information (ESI) available: See DOI:

The water splitting breakthrough reported by Fujishima and Honda is one of the main discoveries that promoted the development of photocatalysis across a broad range of research areas, including especially environmental and energy-related fields.¹⁻³ The photocatalytic properties of certain materials have been used with the ultimate goal of converting solar energy into chemical energy used either to oxidize or to reduce compounds, to obtain useful products including hydrogen and hydrocarbons, and to remove pollutants and bacteria from wall surfaces, and either in air or in water environments.⁴⁻⁵⁶⁷ Among different photocatalysts investigated, titanium dioxide (TiO₂) is a fascinating material exhibiting unique photocatalytic properties which are exploited in many technological applications due to its strong oxidizing abilities for the decomposition of organic pollutants, chemical stability, long durability, nontoxicity and low cost.**¡Error! Marcador no definido.**⁸ The possibility to use sunlight for photocatalytic processes carries the promise to an almost inexhaustible and sustainable energy source and TiO₂, in its many forms, is by far the most studied compound. An earnest effort has been put into designing TiO₂ based photocatalysts for maximizing the quantum efficiency and yields of these photocatalytic systems. Many TiO₂ nanostructures with different morphology such as spheres, nanorods, fibers, tubes, sheets, and interconnected architectures have been recently fabricated.⁹⁻¹³ Not surprisingly, the morphology control together with that of the size of the system are two aspects to be taken into account when aiming at optimizing their photocatalytic activity.¹⁴

Unfortunately, because of many technical problems, it is very difficult to rely on experiments to correlate the effect of size and shape to the electronic properties of TiO₂ nanosystems. On the other hand, computational modeling provides a reliable and unbiased approach to analyze the influence of these factors on the structural and electronic properties. However, the design either of different morphologies keeping the composition or of varying composition for a given morphology requires appropriate realistic models containing perhaps thousands of atoms. Recent works based on bottom-up^{15,16-17} and top-down¹⁸ models of TiO₂ nanoparticles have been reported showing that it is nowadays possible to approach the properties of realistic systems by means of first principles density functional theory (DFT) based calculations. These works have shown how electronic properties of TiO₂ finite systems such as the optical gap (O_{gap}), corresponding to the lowest singlet to singlet excitation, and electronic gap (E_{gap}), defined as the difference between vertical ionization potential and electron affinity, evolve with the morphology of the material.**¡Error! Marcador no definido.¡Error! Marcador no definido.** The largest variations are, not surprisingly, observed in the quite small (TiO₂)_n nanoclusters with $n < 30$.**¡Error! Marcador no definido.** These fluctuations result from quantum confinement and atomic environments which are far enough away from the bulk atomic connections.

For fairly large nanoparticles of ~6nm and containing more than one thousand atoms, O_{gap} and E_{gap} values are larger than those predicted for the bulk phases using the same computational approach.**¡Error! Marcador no definido.** Nevertheless, a monotonous trend on O_{gap} and E_{gap} converging to

the bulk like values as the size increases is observed and it also concluded that $(\text{TiO}_2)_{84}$ nanoparticles can be considered at the onset of the so-called scalable regime where properties scale linearly with size toward bulk like limit. This behavior is systematically observed with similar trend for semilocal and hybrid exchange-correlation functionals. The inclusion of the Fock exchange through PBE_x (PBE¹⁹ with 12.5% Fock) and PBE0 (PBE with 25% Fock) leads to larger value of both O_{gap} and E_{gap} contribution and, in the view of the results reported for bulk phases,²⁰ are expected to provide more accurate results even if the trends observed with the PBE functional are maintained. The origin of the up-shifts in the PBE calculated O_{gap} is associated to systematic errors as recently reported for a large database of extended solids.²¹ In particular, a linear correlation was found between the PBE and G_0W_0 calculated O_{gap} values, the latter matching nicely experimental values. Note in passing by that, in absence of excitons, O_{gap} and E_{gap} in extended solids coincide. Interestingly, the correlations above indicate that the problem of predicting the band gap from standard DFT calculations arises from the incorrect assignment of quasiparticle character to the Kohn-Sham energy levels. The correlation also indicates that taking the Kohn-Sham bands to estimate the band gap carries a systematic error that can be corrected by invoking this correlation. The question that naturally arises is whether this systematic error also holds for TiO_2 nanoparticles since in that the case it would be possible to estimate the energy gap of sufficiently large nanoparticles better mimicking the synthesized ones.

In this communication, we investigate whether the correlation found for PBE and PBE_x calculated O_{gap} values on periodic insulators or semiconductors, and hence between PBE and G_0W_0 and, consequently, between PBE and experiment also holds for TiO_2 finite systems. To this end we study many different morphologies such as spherical, octahedral, lamellar, or tubular finite structures (further structural details can be found in refs. 15 and 17). The O_{gap} is estimated from the HOMO-LUMO energy gap defined from the Kohn-Sham orbital energies since, even if it cannot be considered as a reliable approximation to this quantity, detailed studies at the G_0W_0 level of theory have shown that the trends are meaningful.²² A set of 75 different $(\text{TiO}_2)_n$ finite systems with n ranging from 10 to 286 units has been selected and classified in two groups attending to the number of TiO_2 units: (i) nanoclusters ($n \leq 40$) obtained by using a bottom-up approach based on hybrid genetic algorithm and global optimization, and (ii) nanoparticles ($n > 40$) which are obtained by using a top-down approximation via Wulff constructions.²³ Note that the top-down approach allows one to relate the shape of the nanoparticle with the area of the surfaces exposed concerning their relative stability. Rutile and anatase bulk phases were used to design nanoparticles containing up to 1689 atoms.²⁴ As an example, Figure 1 compiles a set of six TiO_2 nanoclusters and nanoparticles representing the rich variety of sizes and shapes analyzed in the present study.

Calculations reported in the present work for the series of nanoparticles described above explicitly include all electrons, and the electron density is described through a numerical atom-centered (NAO) orbital basis set, as implemented in the Fritz Haber Institute *ab initio* molecular simulations (FHI-aims) code which shows a linear scaling with the number of cores for systems composed by thousands of atoms.²⁵ The light grid and tier-1 basis set are selected which lead to a quality comparable to that corresponding to a Gaussian Type Orbital TZVP basis set. **Error! Marcador no definido.** The convergence threshold for atomic forces in relaxation of TiO₂ nanoclusters and nanoparticles is set to 10⁻² eV Å⁻¹. Relativistic effects are also included through the zero-order regular approximation (ZORA).^{26,27}

We start with the analysis of the PBE or PBEx calculated O_{gap} of TiO₂ nanoclusters ($n = 10-40$). Recall that within this size range O_{gap} depends strongly on the nanocluster morphology, which is clearly shown by the wide range of O_{gap} reported, 1.80–3.60 eV ($\Delta=1.80$ eV) calculated by using the PBE functional. This variation on the O_{gap} also affects TiO₂ nanocluster isomers with different morphologies. For instance, three different (TiO₂)₁₈ nanoclusters were analyzed reporting a O_{gap} running from 1.92 to 3.01 eV or similarly the case of other three different (TiO₂)₄₀ ones which go from 2.09 to 2.94 eV (see Tables S1 and S2 in ESI†). PBEx results show similar tendencies, but the range of O_{gap} is quantitatively increased up to 3.01-4.87 eV ($\Delta=1.86$ eV) due to the inclusion of the Fock contribution. In the light of PBEx hybrid functional containing the appropriate percent of exchange Fock contribution, O_{gap} values are significantly larger than those of anatase and rutile bulk phases, 3.2 and 3.0 eV, respectively (see Tables S1 and S2 in the ESI†). These large differences depending on TiO₂ nanocluster are associated with the system size, which is well away from the bulk limit region. This is consistent with previous findings that indicate that very large TiO₂ nanoparticles composed by hundreds of TiO₂ units are required to obtain realistic models with electronic properties close to bulk like, consistent with the experimental evidences.

Realistic (TiO₂)_n nanoparticles with octahedral ($n=84, 165$ and 286) and truncated octahedral ($n=78, 97$ and 151) shapes (see Figure 1 and Table S3 in ESI†) terminated so as to exhibit the most stable (101) and (001) **Error! Marcador no definido.** surfaces of TiO₂ anatase are considered. For this set of nanoparticles, the PBE O_{gap} tends to the anatase PBE bulk phase value by increasing the nanoparticle size ($n \sim \infty$). TiO₂ nanoparticles with octahedral shape have PBE O_{gap} values of 2.52 eV for (TiO₂)₈₄, a value decreasing to 2.32 eV for (TiO₂)₂₈₆. Using the PBEx functional shifts these values up to 3.56 and 3.46 eV, respectively, values converging to the PBEx anatase band (3.2 eV), although still large. An analogous tendency is observed for the TiO₂ truncated octahedral shape, where PBE O_{gap} values of 2.46 and 2.38 eV are predicted for (TiO₂)₇₈ and (TiO₂)₁₅₁, respectively, which become 3.61 and 3.51 eV when using the PBEx functional (see Table S3 in the ESI†). The case of rutile nanoparticles ($n=86, 111$ and 211) is more complex because (110), (101) and (100) surfaces must be considered for designing the nanoparticles. **Error! Marcador no definido.** The PBE O_{gap} values for (TiO₂)₁₁₁ and (TiO₂)₂₁₁ are 1.71 and 1.66 eV, respectively, whereas the PBEx value are 2.76 and 2.71 eV. The latter values tend to the energy

gap of the rutile bulk phase (3.0 eV). In summary, realistic TiO₂ nanoparticles visualize clearly the trend of O_{gap} towards the bulk like regime whereas TiO₂ nanoclusters behave differently, as expected.

Next we analyze the correlation between the PBE and PBEx calculated O_{gap} values which is reported in Figure 2. A quantitatively enough linear correlation between both sets of calculated O_{gap} values emerges as in Eq. (1),

$$O_{\text{gap}}(\text{PBEx}) = 0.995 \cdot O_{\text{gap}}(\text{PBE}) + 1.253 \quad (1)$$

with a regression coefficient of 0.98. This correlation confirms that the Fock contribution to the exchange induces a systematic opening of the Kohn-Sham HOMO and LUMO orbital energies for the set of TiO₂ nanoclusters and nanoparticles. Interestingly enough, this systematic effect is observed for any nanoparticle with any morphology and any size. The offset value of 1.25 eV is consistent with the existence of a systematic deviation on the PBE results for O_{gap} that we attribute to interpretation of Kohn-Sham orbital energies as quasiparticle excitation. It should be pointed out that this linear correlation allows one to predict PBEx O_{gap} values of any TiO₂ nanoparticle composed by hundreds/thousands of TiO₂ units where the use of hybrid functional is computationally unfeasible. Thus, we provide here a suitable way to predict the O_{gap} of realistic TiO₂ nanoparticles with a PBEx precision just carrying out a single point calculation with the PBE functional. Moreover, in the view of the (by construction) coincidence between PBEx and experiment for bulk phases, it is possible to argue that PBE O_{gap} and Eq. (1) will provide a reliable value of this important quantity. For instance, for the anatase (TiO₂)₄₅₅ and rutile (TiO₂)₅₆₃ nanoparticles PBE O_{gap} values reported in Table 1 plus Eq. (1) leads to predicted PBEx O_{gap} values of 3.46 and 2.94 eV for (TiO₂)₄₅₅ and (TiO₂)₅₆₃, respectively. The explicit calculation of these particles at the PBEx level remains unfeasible, or too costly, even with appropriate codes and the modern highly parallel supercomputers with thousands of cores.

To end up the discussion, we focus on the effect of the Fock exchange in the PBEx hybrid functional to the energy of HOMO and LUMO orbitals. Obviously, the opening of energy gap in going from PBE to PBEx is accompanied by changes on the energy of Kohn-Sham orbitals. Figure 3 depicts the PBEx HOMO and LUMO orbital energies against PBE ones. As in the case of O_{gap} (Figure 2), a linear correlation is found for the HOMO orbital energy as in Eq. (2),

$$\text{HOMO}(\text{PBEx}) = 0.986 \cdot \text{HOMO}(\text{PBE}) - 0.947 \quad (2)$$

with a regression coefficient of 0.96 consistent with a second linear correlation for the LUMO orbital energy as in Eq. (3),

$$\text{LUMO}(\text{PBEx}) = 1.031 \cdot \text{LUMO}(\text{PBE}) + 0.497 \quad (3)$$

with a regression coefficient of 0.97. The slope of both fittings is close enough to 1 so as to conclude that the effect of Fock exchange is larger for the HOMO orbitals than LUMO ones. This is clearly observed in Figure 3 by the shifting of both linear tendencies with respect to the ideal correlation; HOMO correlation is further away from it than LUMO one. From Eqs. (2-3) one can predict the PBEx energy of HOMO and LUMO orbitals as reported in Table 1 for $(\text{TiO}_2)_{455}$ and $(\text{TiO}_2)_{563}$ nanoparticles introduced earlier. The resulting O_{gap} values are 3.39 and 2.86 eV for $(\text{TiO}_2)_{455}$ and $(\text{TiO}_2)_{563}$, respectively. Note that the energy gap difference between these O_{gap} values and those obtained by using Eq. (1) is less than 0.1 eV (see Table 1) showing the consistency between both correlations to estimate O_{gap} .

In summary, the optical gap (O_{gap}) in TiO_2 nanoclusters and nanoparticles has been investigated by making use of all electron relativistic DFT based calculations employing the PBE semilocal functional and the hybrid PBEx containing 12.5% of Fock exchange. The present results provide further evidence that O_{gap} is a morphology-dependent property and its value depends on the system size. Small $(\text{TiO}_2)_n$ nanoclusters ($n = 10\text{--}40$) have O_{gap} much larger than corresponding bulk values predicted with the same functional. These large differences are reduced by moving from nanoclusters to realistic nanoparticles which show a bulk like trend consistent with previous studies. **Error! Marcador no definido.**

The present study shows that irrespective of size and morphology, the PBEx hybrid functional induces a systematic gap opening of 1.25 eV for the set of TiO_2 nanoclusters and nanoparticles investigated. The linear correlation found between PBEx and PBE O_{gap} values allows one to predict PBEx quality energy gaps for those TiO_2 finite systems whose dimensionality makes the explicit calculation with hybrid functionals unaffordable. We have further investigated the accuracy of the correlation by fitting the energy gaps for nanoparticles with $n < 80$ only and predicting those of the largest nanoparticles. The comparison between calculated and predicted PBEx O_{gap} values shows a mean absolute error (MAE) below 0.2 eV (see Figures S1, S2 and Table S5 in ESI†). Similar linear trends are observed on HOMO and LUMO orbitals and hence, both orbital energies can be predicted following their trends shown in Eqs. (2-3). The percent of Fock exchange in the hybrid functional has a higher contribution to the HOMO orbitals than to the LUMO ones which promotes a larger downshift on HOMO orbital than the upshift on LUMO one.

Results in the present work show that is possible to obtain a PBEx description of the electronic structure of realistic TiO_2 nanoparticles from the computationally affordable PBE results. It also suggests that similar correlations will exist with other hybrid functionals such as the well known B3LYP and PBE0 and it is in line with previous work highlighting the existence of similar correlation for the electronic gap as predicted from PBE or G_0W_0 calculations. **Error! Marcador no definido.** All together, one can firmly affirm that well-known deviations in the electronic structure properties of nanosized and bulk semiconducting materials predicted by functionals within the gradient generalization approach relative to

those predicted from more accurate hybrid functional or many body based GW approaches are systematic and as such it should be possible to come out with improved and more accurate density functionals.

The authors acknowledge funding from the Spanish *Ministerio de Economía y Competitividad* (MEC) CTQ2015-64618-R grant, partly by *Generalitat de Catalunya* grants 2017SGR13 and XRQTC, and the NOMAD Center of Excellence project, which received funding from the European Union's Horizon 2020 research and innovation programme under grant agreement no. 676580. A. M.-G. thanks the Spanish MEC for the *Juan de la Cierva* (FJCI-2015-23760) postdoctoral grant. F. I. acknowledges additional support from the 2015 ICREA Academia Award for Excellence in University Research. Computational time at the MareNostrum supercomputer has been provided by the Barcelona Supercomputing Centre (BSC) through grants from *Red Española de Supercomputación* (RES) and the EXCIPHOCAT project under grant no. 2016163940 of the Partnership for Advanced Computing in Europe (PRACE).

Conflict of interest

There are no conflicts to declare.

Table 1. O_{gap} for anatase $(\text{TiO}_2)_{455}$ and rutile $(\text{TiO}_2)_{563}$ nanoparticles calculated by using PBE functional. The predicted O_{gap} with a PBE accuracy is calculated by using Eqs. (1-3). $|\Delta|$ stands for the difference between the predicted O_{gap} (PBE) by using Eq. (1) and that predicted by using the estimated PBE LUMO–HOMO difference from Eqs. (2) and (3), respectively.

		Anatase	Rutile
		$(\text{TiO}_2)_{455}$	$(\text{TiO}_2)_{563}$
PBE	HOMO	-7.465	-7.247
	LUMO	-5.253	-5.558
	O_{gap}	2.212	1.689
Predicted PBE	HOMO Eq. (2)	-8.308	-8.093
	LUMO Eq. (3)	-4.919	-5.233
	O_{gap}	3.389	2.859
	O_{gap} Eq. (1)	3.465	2.942
	$\Delta (O_{\text{gap}})$	0.076	0.083

Fig 1. Representative scheme of $(\text{TiO}_2)_n$ nanoclusters ($n=20, 28$ and 64) and nanoparticles ($n=151, 211$ and 286). Nanoclusters and nanoparticles are obtained by using bottom-up and top-down approaches, respectively. $(\text{TiO}_2)_{151}$ is structurally described as an anatase-type truncated octahedral nanoparticle. $(\text{TiO}_2)_{211}$ is a rutile-type polyhedral nanoparticle, and finally $(\text{TiO}_2)_{286}$ is also an anatase-type octahedral nanoparticle.

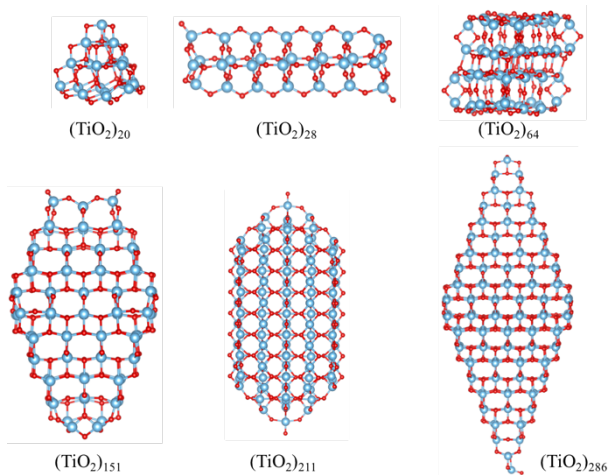


Fig 2. Correlation between $O_{\text{gap}}(\text{PBEx})$ and $O_{\text{gap}}(\text{PBE})$ for the set of 75 $(\text{TiO}_2)_n$ nanocluster/nanoparticles. O_{gap} is taken as the HOMO-LUMO gap which corresponds to the Kohn-Sham orbital energies. The point-dashed line corresponds to an ideal correlation $y = x$ and the yellow line to the linear fitting.

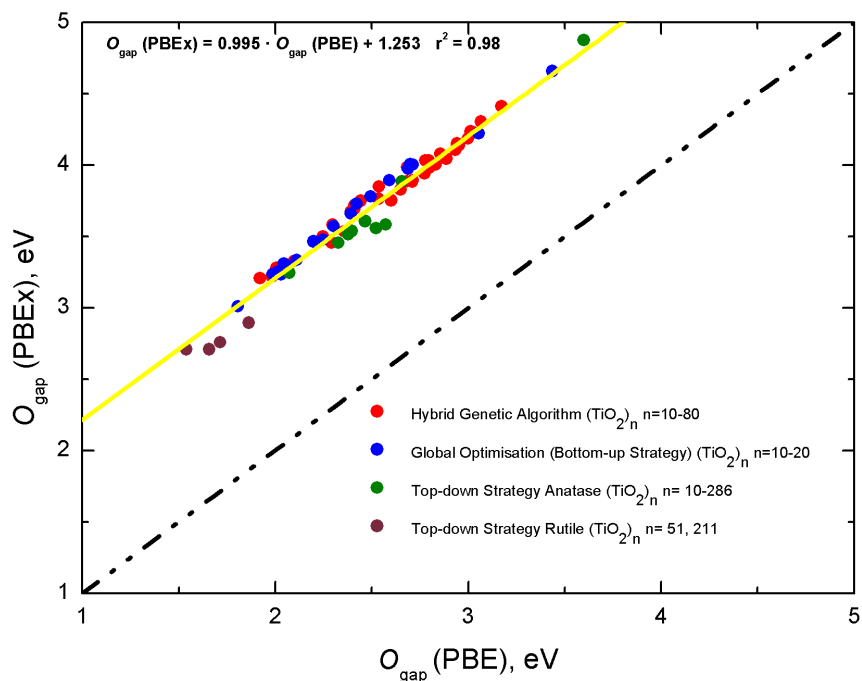
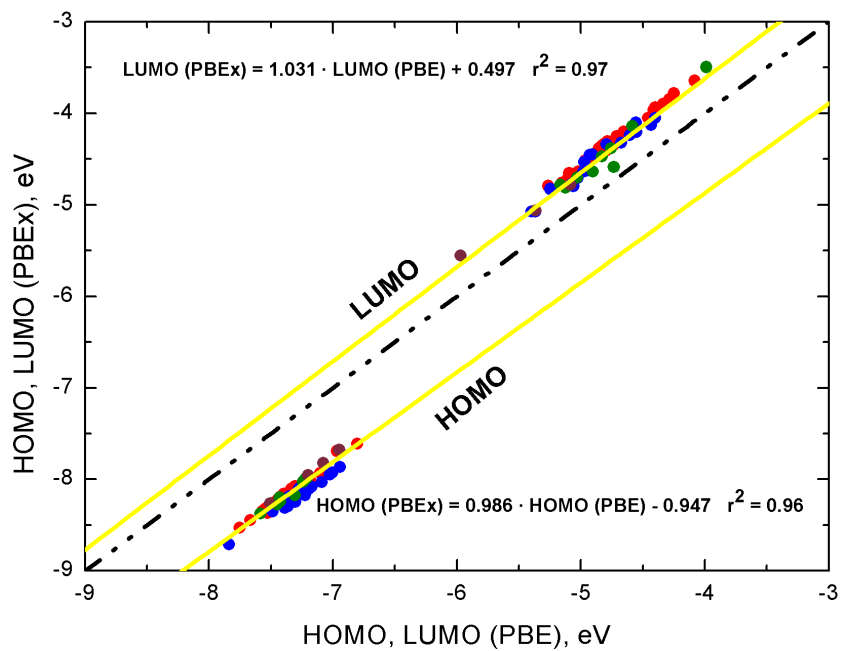


Fig 3. Correlation between HOMO and LUMO Kohn-Sham orbital energies of PBEx and PBE functionals for the set of 75 $(\text{TiO}_2)_n$ nanocluster/nanoparticles. The color scheme follows the same notation as reported Figure 2 inset. The point-dashed line corresponds to an ideal correlation $y = x$ and yellow lines to linear fittings.



References

- (1) A. Fujishima, K. Honda, *Nature*, 1972, **238**, 37-38.
- (2) K. Hashimoto, H. Irie, A. Fujishima, *Jpn. J. Appl. Phys.*, 2005, **44**, 8269-8285.
- (3) A. Fujishima, X. Zhang, D. A. Tryk, *Surf. Sci. Rep.*, 2008, **63**, 515-582.
- (4) A. Ryu, *J. Photochem. Photobiol. C*, 2010, **11**, 179-209.
- (5) T. Inoue, A. Fujishima, S. Konishi, K. Honda, *Nature*, 1979, **277**, 637-638.
- (6) L. Caballero, K. A. Whitehead, N. S. Allen, J. Verran, *J. Photochem. Photobiol. A*, 2009, **202**, 92-98.
- (7) K. Sunada, T. Watanabe, K. Hashimoto, *Environ. Sci. Technol.*, 2003, **37**, 4785-4789.
- (8) H. Xu, S. Ouyang, L. Liu, P. Reunchan, N. Umezawa, J. Ye, *J. Mater. Chem. A*, 2014, **2**, 12642-12661.
- (9) J. S. Chen, Y. L. Tan, C. M. Li, Y. L. Cheah, D. Luan, S. Madhavi, F. Y. C. Boey, L. A. Archer, X. W. Lou, *J. Am. Chem. Soc.*, 2010, **132**, 6124-6130.
- (10) X. Feng, J. Zhai, L. Jiang, *Angew. Chem. Int. Ed.*, 2005, **44**, 5115-5118.
- (11) Y. Cheng, W. Huang, Y. Zhang, L. Zhu, Y. Liu, X. Fan, X. Cao, *Cryst. Eng. Comm.*, 2010, **12**, 2256-2260.
- (12) J. M. Macak, M. Zlamal, J. Krysa, P. Schmuki, *Small*, 2007, **3**, 300-304.
- (13) T. Shibata, N. Sakai, K. Fuduka, Y. Ebina, T. Sasaki, *Phys. Chem. Chem. Phys.*, 2007, **9**, 2413-2420.
- (14) X. Chen, S. S. Mao, *Chem. Rev.*, 2007, **107**, 2891-2959.
- (15) O. Lamiel-García, A. Cuko, M. Calatayud, F. Illas, S. T. Bromley, *Nanoscale*, 2017, **9**, 1049-1058.
- (16) D. Cho, K. C. Ko, O. Lamiel-García, S. T. Bromley, J. Y. Lee, F. Illas, *J. Chem. Theory Comput.*, 2016, **12**, 3751-3763.
- (17) M. Chen, D. A. Dixon, *Nanoscale*, 2017, **9**, 7143-7162.
- (18) O. Lamiel-García, K. C. Ko, J. Y. Lee, S. T. Bromley, F. Illas, *J. Chem. Theory Comput.*, 2017, **13**, 1785-1793.

- (19) J. P. Perdew, K. Burke, M. Ernzerhof, *Phys. Rev. Lett.*, 1996, **77**, 3865-3868.
- (20) K. C. Ko, O. Lamiel-García, J. Y. Lee, and F. Illas, *Phys. Chem. Chem. Phys.*, 2016, **18**, 12357-123667
- (21) A. Morales-García, R. Valero, F. Illas, *J. Phys. Chem. C*, 2017, **121**, 18862-18866.
- (22) A. Morales-García, R. Valero, F. Illas, *J. Chem. Theory Comput.*, 2017, **13**, 3746-3753.
- (23) G. Wulff, *Z. Kristallogr.*, 1901, **34**, 449-530.
- (24) K. C. Ko, S. T. Bromley, J. Y. Lee, F. Illas, *J. Phys. Chem. Lett.*, 2017, **8**, 5593-5598.
- (25) V. Blum, R. Gehrke, P. Hanke, P. Havu, V. Havu, X. Ren, K. Reuter, M. Scheffler, *Comput. Phys. Commun.*, 2009, **180**, 2175-2196.
- (26) C. Chang, M. Pelissier, M. Durand, *Phys. Scr.*, 1986, **34**, 394-404.
- (27) E. van Lenthe, R. van Leeuwen, E. J. Baerends, J. G. Snijders, *Int. J. Quantum Chem.*, 1994, **57**, 281-293.

TOC

